Anisotropic Reflectance Correction of SPOT-3 HRV Imagery

By: Jeffrey D. Colby

Abstract: The problem of anisotropic reflectance in mountainous terrain is well known. It was required to determine the efficacy of anisotropic reflectance correction (ARC) of imagery acquired over the western Himalaya. The Minnaert correction procedure was evaluated using a single Minnaert constant (k), locally computed ks and land cover-computed ks. Findings illustrate the need for computing ks, such that anisotropic reflectance caused by topography and land cover is accounted for. This resulted in a significant reduction in the topographic effect. The results indicate that land cover-computed k values can be used effectively for anisotropic reflectance correction.

Bishop, M.P., and **Colby, J.D.** (2002). Anisotropic Reflectance Correction of SPOT-3 HRV Imagery. International Journal of Remote Sensing, 23(10):2125-2131. (May 20, 2002) Published by Taylor & Francis (ISSN: 1366-590). DOI: 10.1080/01431160110097231

Anisotropic reflectance correction of SPOT-3 HRV imagery

(*Received 13 July 2000; in final form 3 July 2001*)

Abstract. The problem of anisotropic reflectance in mountainous terrain is well known. It was required to determine the efficacy of anisotropic reflectance correction (ARC) of imagery acquired over the western Himalaya. The Minnaert correction procedure was evaluated using a single Minnaert constant (k), locally computed ks and land cover-computed ks. Findings illustrate the need for computing ks, such that anisotropic reflectance caused by topography and land cover is accounted for. This resulted in a significant reduction in the topographic effect. The results indicate that land cover-computed k values can be used effectively for anisotropic reflectance correction.

1. Introduction

The use of remotely sensed data in mountain environments is problematic because of variations in the irradiant and radiant flux caused by the atmosphere, topography, and land cover (Hugli and Frei 1983). Earth scientists have recognized this problem and have developed anisotropic reflectance correction (ARC) procedures to reduce the topographic effect in imagery.

To date, no one procedure has emerged as suitable for operational ARC. Several investigators have reported on the potential of the Minnaert correction procedure, although it does not adequately account for anisotropic reflectance caused by land cover. Therefore, more research is warranted.

This research was designed to evaluate the Minnaert correction procedure for ARC of satellite imagery acquired at Nanga Parbat, in northern Pakistan. Specific objectives were to evaluate the use of:

1. a single globally computed Minnaert constant (k);
2. locally computed ks;
3. land cover-computed ks.

2. Study area

Nanga Parbat mountain is the ninth largest in the world at 8125 m. Slope angles are steep at all altitudes, and the relationship between slope angle and altitude is

nonlinear. This region is geologically active, and rapid tectonic uplift and ferocious denudation produces extreme relief and complex topography (Bishop and Shroder 2000). River incision, glaciation and mass movement are the dominant surface processes, and a strong climatic gradient is present. Land cover characteristics are highly variable and consist of igneous and metamorphic rocks, glacial till, sagebrush, temperate coniferous forest, subalpine forest, tundra, and permanent snow and ice.

3. Methodology

3.1. *Data*

A SPOT-3 HRV near-infrared image was used for analysis. Multispectral data were acquired on 9 June 1996. Solar geometry parameters were 71.2° and 127.0° for solar elevation and azimuth respectively. The sensor incident angle was left at 0.9°, which equates to near-nadir viewing. SPOT-3 HRV panchromatic stereopairs were also obtained to generate a DEM. The image was ortho-rectified with a rms error of ± 5 m.

The digital numbers were transformed to radiance using the equation by Yang and Vidal (1990):

$$L = \frac{DN}{\alpha} \tag{1}$$

where L is the radiance {W m^{-2}sr^{-1} μm^{-1}}, DN is the digital number {0–255}, and α is the absolute calibration coefficient {W m^{-2}sr^{-1} μm^{-1}}.

3.2. *Anisotropic reflectance correction*

The cosine correction procedure assumes that reflectance variability is primarily caused by local topographic properties, where radiance is proportional to the cosine of the incidence angle (i):

$$\cos i = \cos\theta_s \cos(\beta_t) + \sin\theta_s \sin\beta_t \cos(\phi_t - \phi_s) \tag{2}$$

where θ_s is the solar zenith angle, β_t is the slope angle of the terrain, ϕ_s is the solar azimuth angle, and ϕ_t is the slope aspect angle of the terrain.

The Minnaert correction procedure was implemented using the general backwards radiance correction procedure described by Colby (1991):

$$L_\lambda^n = (L_\lambda \cos e)/(\cos^k i \cos^k e) \tag{3}$$

where e is the exitant angle ($e = \beta_t$). Minnaert constants were calculated using least-squares regression on the variables x and y, where $x = \log(\cos i \cos e)$ and $y = \log(L_\lambda \cos e)$. The slope of the regression equation represents k.

L_λ^n was generated using the following spatial implementation options for computing k.

1. Globally computed k. Entire image used.
2. Locally computed ks. A sliding-window approach to computing a local k value for each pixel. An arbitrary range of window sizes was used to determine how window size would affect the results (11×11, 21×21, 101×101, and 201×201). This was done to address previous research that indicated the need to evaluate local Minnaert constants (Colby 1991).
3. Land cover-computed ks. The image was classified into three primary classes of snow, vegetation, and nonvegetation using thresholding and automated

ISODATA cluster analysis of the NDVI image. The classification depicted the vertical zonation associated with the climate gradient at Nanga Parbat. The map served as the basis for stratified regression analysis. The emphasis here is not on classification accuracy, but on stratification for the generation of high r^2 values in computing ks.

3.3. *ARC assessment*

Two-dimensional semivariogram analysis was used, where every pixel was compared to every other pixel in a subarea. Within an $n_x \times n_y$ grid there will be N point pairs, where $N = n_x^2(n_y^2 - 1)/2$. The variance component is $\Delta L = (L_1 - L_2)^2$, and the horizontal distance is $\Delta x = \{(x_1 - x_2)^2 + (y_1 - y_2)^2\}^{0.5}$. The variance was summed over a binned horizontal distance interval (20 m) and divided by the number of observations within each bin to calculate the average semivariance (S^2).

Effective ARC should result in an image that exhibits less spectral variation at lag distances where topography increases spectral variability, and greater spectral variation at lag distances associated with land cover variation.

4. Results and discussion

4.1. *Cosine correction*

The cosine corrected image ($L/\cos i$) exhibited high radiance values that were associated with steep slopes (figures 1 and 2). This procedure does not effectively take other irradiance components into consideration, resulting in overcorrection, as steep slopes receive irradiance from the atmosphere and the adjacent terrain. Semivariograms revealed that the correction procedure increased spectral variation at all lag distances. These results indicate that the cosine correction procedure has limited utility for ARC given steep slopes and extreme relief.

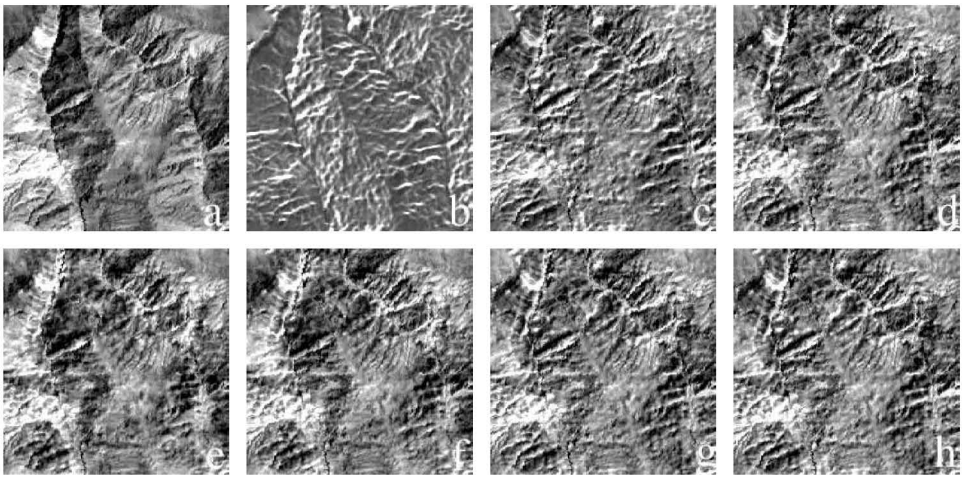

Figure 1. Subimages of a 200×200 pixel area of the Raikot Fault Zone that represent (a) SPOT-3 HRV NIR image; (b) cosine correction; (c) NLMG-(global k); (d) NLM3-(land cover ks); (e) NLM11-(11×11window); (f) NLM21-(21×21window); (g) NLM101-(101×101window); (h) NLM201-(201×201window).

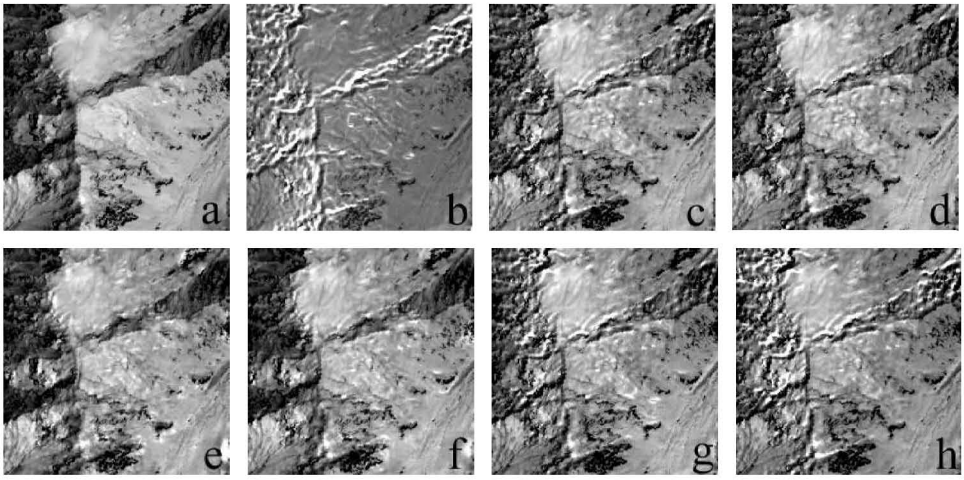

Figure 2. Subimages of a 200×200 pixel area at Buldar Peak that represent (a) SPOT-3 HRV NIR image; (b) cosine correction; (c) NLMG-(global k); (d) NLM3-(land cover ks); (e) NLM11-(11×11window); (f) NLM21-(21×21window); (g) NLM101-(101×101window); (h) NLM201-(201×201window).

4.2. *Minnaert correction–globally computed* k*s*

Regression analysis yielded a Minnaert constant and r^2 value of 0.5234 and 0.123 respectively. Visual interpretation indicated that the influence of topography was reduced (figures 1 and 2), although high radiance values were found at the base of steep slopes. This was verified by finding a nonlinear relationship between L_λ^n and $\cos i$.

Semivariograms over the Raikot Fault Zone area indicated that the correction procedure increased the spectral variation at all lag distances (figure 3). Conversely, at Buldar peak, the correction procedure decreased spectral variation at lag distances >0.4 km (figure 4).

The low r^2 value indicated that k cannot be used to effectively characterize anisotropic reflectance caused by land cover. Consequently, this approach is problematic for areas that exhibit heterogeneous land cover conditions and complex topography. Complex mountain environments dictate that a low r^2 value will result when computating k. This does not preclude the generation of a high r^2 value for areas that exhibit moderate topography and homogeneous land cover characteristics. These results indicate that this approach cannot be used for operational ARC.

4.3. *Minnaert correction–locally computed* k*s*

Small window sizes produced highly variable r^2 values, such that the corrected images did not exhibit a reduction in spectral variation caused by the topography (figure 2). Semivariograms indicated that the correction procedure did not significantly reduce spectral variation at various lag distances (figures 3 and 4). These results indicate that local ks do not accurately characterize anisotropic reflectance conditions within such a small area.

Conversely, the use of the two larger window sizes resulted in corrected images that exhibited a decrease in spectral variation at lag distances >0.4 km (figures 3 and 4). For the Raikot Fault Zone, r^2 values were on average $\geqslant 0.7$, and the corrected images highlight the structural and lithological variations of the metasedimentary

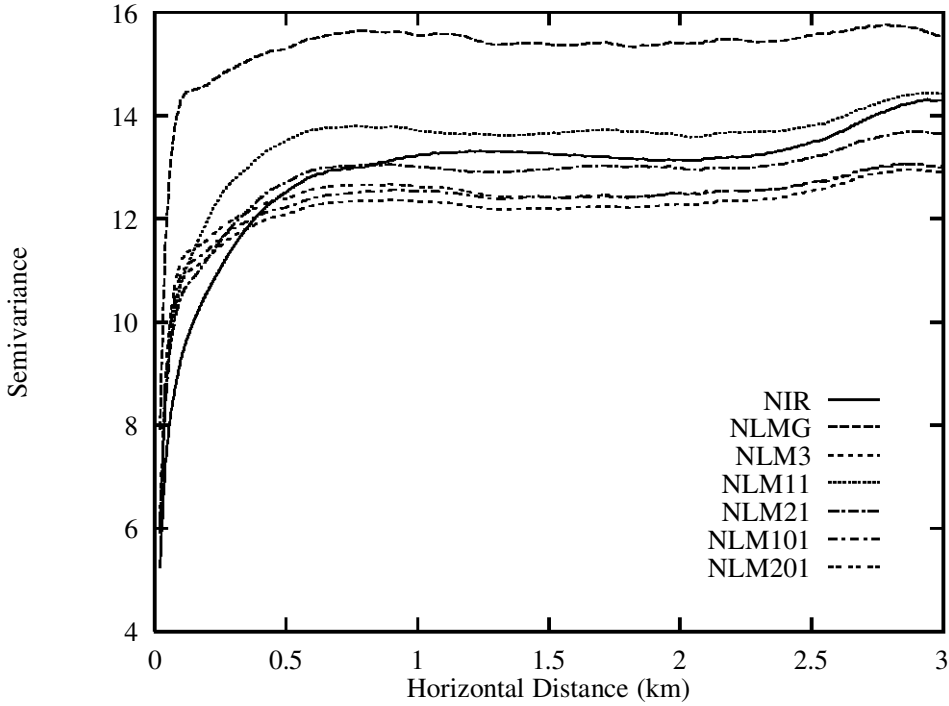

Figure 3. Semivariograms for the Raikot Fault Zone depicted in figure 1.

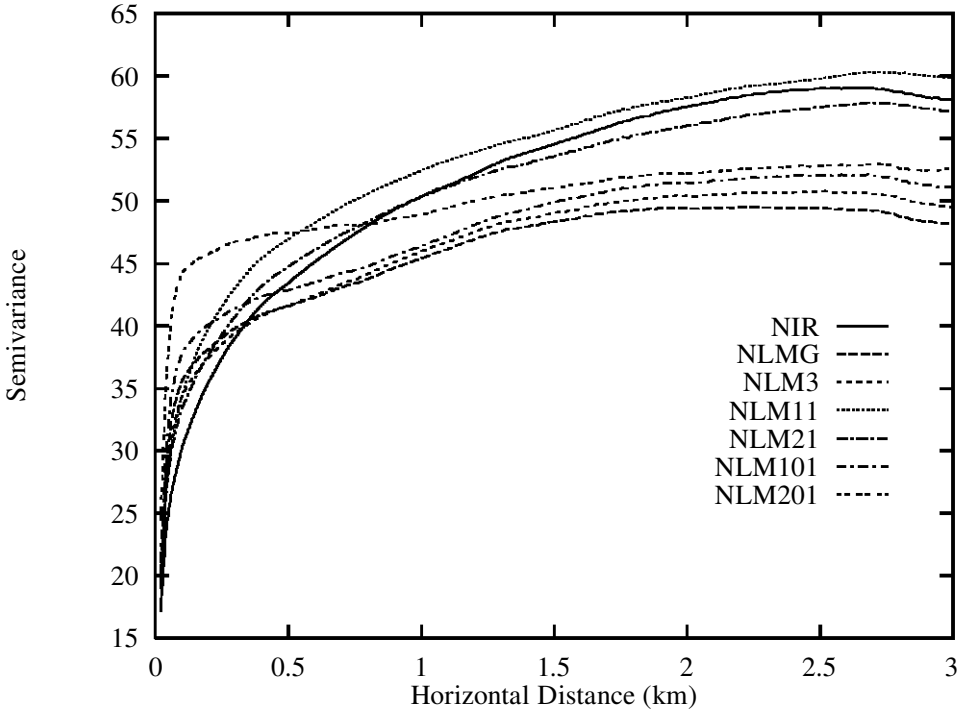

Figure 4. Semivariograms for Buldar Peak depicted in figure 2.

sequences. This was not the case at Buldar Peak, however, as low r^2 values were the result of snow and non-snow classes being sampled and used for the computation of k.

Theoretically, this approach can account for anisotropic reflectance caused by land cover and topography. Small windows, however, do not capture enough topographic variation to generate high r^2 values, while the use of larger window sizes will sample multiple land cover classes. In practice, this approach is limited by the need for *a priori* knowledge of the spatial structure of the landscape.

4.4. *Minnaert correction–land cover-computed* k*s*

Image stratification resulted in a classification that depicted snow, vegetation, and nonvegetation features. Stratified regression analysis resulted in three k values (table 1).

This implementation resulted in a corrected image that exhibited reduced spectral variation at lag distances >0.4 km, and higher spectral variation at lag distances <0.4 km (figures 3 and 4). This approach addresses the problems associated with using a single k value, as the spatial structure of land cover is used to compute ks.

This approach enables hierarchical clustering to be utilized to produce more classes which would increase the magnitude of r^2 values associated with different land cover classes. More research regarding the use of better stratification methods is warranted.

5. Conclusions

1. The Minnaert correction procedure and a single k value cannot be used for operational ARC.
2. The use of locally computed ks produced inconsistent results. This spatial implementation option dictates the computation of ks with low r^2 values.
3. Land cover-computed ks can be generated with relatively high r^2 values. This approach resulted in ARC which reduced the topographic effect and increased the spectral variation among land cover classes.
4. ARC procedures alter the spatial variance structure of images. Consequently, visual interpretation, classification accuracies, and examination of $L^n - \cos i$ scatterplots are not recommended as diagnostic assessment procedures for determining the validity of ARC results.

Acknowledgments

This work was funded by the University Committee on Research at the University of Nebraska at Omaha, the National Science Foundation (Grant No. EAR 9418839 and EPS-9720643), and East Carolina University, College Research Award.

Table 1. Land cover stratified regression analysis.

Class	k	r^2	n
Nonvegetation	0.4052	0.4081	1 266 086
Vegetation	0.4437	0.5182	418 362
Snow/Firn	0.4840	0.5757	958 465

References

Bishop, M. P., and Shroder Jr., J. F., 2000, Remote sensing and geomorphometric assessment of topographic complexity and erosion dynamics in the Nanga Parbat massif. In *Tectonics of the Nanga Parbat Syntaxis and the Western Himalaya*, edited by M. A. Khan, P. J. Treloar, M. P. Searle and M. Q. Jan (London: Geological Society), pp. 181–199.

Colby, J. D., 1991, Topographic normalization in rugged terrain. *Photogrammetric Engineering and Remote Sensing*, **57**, 531–537.

Hugli, H., and Frei, W., 1983, Understanding anisotropic reflectance in mountainous terrain. *Photogrammetric Engineering and Remote Sensing*, **49**, 671–683.

Yang, C., and Vidal, A., 1990, Combination of digital elevation models with SPOT-1 HRV multispectral imagery for reflectance factor mapping. *Remote Sensing of Environment*, **32**, 35–45.